Hindawi Publishing Corporation
EURASIP Journal on Wireless Communications and Networking
Volume 2009, Article ID 532474, 8 pages
doi:10.1155/2009/532474

Research Article

Towards a Performance Boundary in Calibrating Indoor Ray Tracing Models

Jaouhar Jemai[1] and Thomas Kürner[2]

[1] *Ubisense AG, Development and Services, 80637 Munich, Germany*
[2] *Institut für Nachrichtentechnik, Technische Universität Carolo-Wilhelmina Braunschweig, 38106 Braunschweig, Germany*

Correspondence should be addressed to Jaouhar Jemai, jaouhar_jemai@hotmail.com

Received 27 July 2008; Revised 18 December 2008; Accepted 20 February 2009

Recommended by Jun-ichi Takada

This paper investigates the performance boundaries of a calibrated deterministic indoor channel model. From a propagation modeling point of view, this process allows to assess the weakness of ray tracing and sets the boundary conditions for a such modeling method. The principle of the deterministic model calibration used in this work focuses upon the estimation of optimal material parameters by means of a few pilot measurements and a simulated annealing method. This technique improves the accuracy of the prediction model for all measurement positions including those not considered by the calibration. The performance of the calibrated ray tracing model and the sensitivity of the calibration to the number of pilot measurements have been investigated. For this investigation, a measurement campaign has been conducted within an indoor office building at 2.45 GHz with 100 MHz bandwidth. Furthermore, the model performance has been compared to empirical indoor models.

1. Objective and Introduction

The blind prediction, based on a priori approximate knowledge of material parameters, often shows an obvious mismatch with the measurements. Even if predicted path loss values are accurate enough like, for example, in [1], time dispersion parameters could show a significant mismatch. Ray tracing-based conventional deterministic modeling methods use geometrically accurate data and rely on tabulated values for the electrical parameters of the building materials. For instance, the authors in [2] made direct measurements of the building materials. However, the material parameters remain approximate and impossible to define accurately for each building, especially when the building materials are a heterogeneous mixture of unknown components, for which no electromagnetic measurement values are available. Therefore, a calibration of these material parameters, reducing the mismatch between the model and the measurements, is required. The issue of deterministic modeling calibration has been addressed in very few works. In [3], only the dielectric constant of each wall have been tuned separately and the gradient method is used to estimate the solution. However, using the gradient method in conjunction with this tuning provides generally a local minimum and does not necessarily provide the optimal solution.

As the relation between power taps and material parameters is a nonlinear combinatorial relationship, the simulated annealing approach used in this paper provides the general optimal solution by simultaneously changing the dielectric constant and loss tangent of all material parameters with a changing step at each range of iterations. The method proposed converges to a global solution and avoids to be dropped into a local minimum as the gradient method does. The performance and robustness of this calibration procedure is analyzed in this paper by means of an indoor measurement campaign within an office building.

This paper is organized as follows. Section 2 presents the ray tracing model. Section 3 investigates the calibration process and the calibration algorithm. Subsequently, the conducted measurement campaigns and the calibration results for an indoor office environment are highlighted in Section 4. Finally, Section 5 addresses the sensitivity of the calibration to the measurements and assesses the boundary of the modeling methods.

2. The Wideband Semideterministic Prediction Model

The prediction model has been presented earlier by the authors in [4–6]. It has been derived by means of two core components; a geometric engine and an electromagnetic engine. While the geometric engine derives the propagation paths based on the accurate information of the 3D building database, the electromagnetic engine computes the propagation mechanisms and integrates the antenna radiation patterns.

The model requires an accurate 3D indoor database with detailed information describing the scattering objects (walls, doors, and windows), their thickness and their dielectric properties. The required building parameters introduced in the database are the relative dielectric constant ε_r and the loss tangent $\tan\delta$. According to their electromagnetic material properties, the structures of the building are classified into N different classes with common dielectric material parameters.

Besides free-space propagation, the propagation tool computes the Fresnel equations, considering multiple reflections and transmission through walls. Depending on whether the antennas is horizontally or vertically polarized, the system considers the corresponding reflection/transmission coefficients and also the angle of departure (AoD) and angle of arrival (AoA) corresponding to each path. Interactions up to the 3rd order reflection have been considered. Many simulations have confirmed that this order provides a compromise between the accuracy of channel parameter (path loss and delay dispersion) and the reasonable computation time, which is also in accordance with [7]. The tool supports as much transmissions as the wave encounters in its propagation path. It accounts for the single diffraction using the uniform theory of diffraction (UTD) [8].

Thus, the channel model could be represented as a power delay profile (PDP) expressed by

$$h(\tau) = \sum_{k=1}^{L_p} \alpha_k \delta(\tau - \tau_k), \tag{1}$$

where P is the number of taps, α_k and τ_k are the power and time of arrival (ToA) of the kth tap. The deterministic channel modeling provides channel characteristics with an infinite bandwidth. Hence, an infinite discrete time resolution is achieved, enabling all MPCs to be resolved. However, as the measurement bandwidth is generally limited, the resolution of the measurement equipment could not enable the detection of all multipath components. Each group of closely spaced MPCs has been represented with a particular tap delay L_p, the power of which is the sum of these MPCs power. The PDP could then be written as

$$h(\tau) = \sum_{k=1}^{L_p} \sum_{n=1}^{k_n} \alpha_{k_n} \delta(\tau - \tau_k), \tag{2}$$

whereby k_n is the number of MPCs clustered together to form the kth tap.

Since typically only 2D radiation patterns (horizontal and vertical) are available, the developed model derives the 3D antenna radiation pattern through a bilinear interpolation knowing the measured 2D patterns in E- and H-planes [9]. Moreover, for a better accuracy, the system model integrates also 3D measured antenna patterns within an anechoic chamber.

3. Model Calibration

The calibration consists in extracting relevant multipath components (MPCs), for instance once reflected paths, simultaneously from the model and measurement. Afterwards, the simulated annealing is performed to optimize the material parameters.

3.1. Extraction of Parameters for Calibration. The measured and predicted PDPs h_{meas} and h_{mod} are given by

$$\begin{aligned} h_{\text{meas}}(\tau) &= \sum_{k=1}^{Lp_{\text{meas}}} (\alpha_k)_{\text{meas}} \delta(\tau - \tau_k), \\ h_{\text{mod}}(\tau) &= \sum_{k=1}^{Lp_{\text{mod}}} (\alpha_k)_{\text{mod}} \delta(\tau - \tau_k). \end{aligned} \tag{3}$$

After identifying the direct path, according to the arrival time corresponding to the distance separating Tx and Rx, particular P power taps (e.g., once reflected paths) with a power above the noise threshold have been extracted from the measurement and the model simultaneously. The noise threshold is computed from each measurement based on a dynamic noise clipping. Hence, two vectors of power taps have been formed which are $[[(\alpha_k)_{\text{meas}}]_{n=1}^{P}]^T$ and $[[(\alpha_k)_{\text{mod}}]_{n=1}^{P}]^T$. The calibration uses the electromagnetic engine, the power tap matrices and the involved building structures to optimize the material parameters incorporated by the deterministic model.

3.2. Simulated Annealing Algorithm: Practical Implementation for Material Parameters Estimation. The "Simulated Annealing" is analogous to the phenomenon of heating a material and letting it cool gradually until reaching a steady state. By the cooling process, the material reaches a global optimum, for which a global minimum energy crystalline structure is dissipated. Starting with an initial solution s (set of material parameters for the N classes) at a relatively high chosen temperature T_0, a neighbor solution s' is afterwards generated as a next solution for which the evolution in cost, $\Delta E(s, s') = E(s') - E(s)$, is evaluated. If the cots decreases, the generated neighbor solution becomes the current one, otherwise the algorithm decides with a certain probability whether s remains or s' becomes the current solution. The probability of accepting a transition, causing a decrease $\Delta E(s, s')$ in the cost, is called the acceptance function and is set to $e^{-\Delta E/T}$. T is the parameter that corresponds to temperature in the analogy with the physical annealing process. The algorithm runs L steps with the same

Table 1: Simulated annealing algorithm parameters.

Notation	Meaning
s	A random solution as a set of material parameters
$E(s)$	Objective function
T_0	Initial temperature of the stepped geometric decrease
A	Geometric decrease coefficient
L	Number of steps running with constant temperature
ST	Maximum steps the algorithm runs without many changes

temperature. Afterwards, the changing step of the parameters is decreased geometrically with the factor A towards zero. The process is stopped after ST steps if the objective function remains unchanged. The final solution is considered as the absolute optimum. The four configuration parameters (T_0, A, L, and ST) considered by the algorithm are described in Table 1.

The initial material properties are defined using tabulated values available in literature and knowledge of the construction material category. The electromagnetic properties of some different conventional building materials, for example, at the WLAN frequencies can be found in literature [2, 10, 11]. However, some materials are a mixture of unknown components, for which no electromagnetic measurement values are available. Therefore, the optimization process starts from a common value for all these materials, corresponding, for example, to the concrete ($\varepsilon_r = 4.95$, $\tan\delta = 0.01$) at ambient temperature as measured in [11]. The optimized objective (cost) function is defined as the root mean square error between the measured and the predicted tap powers for all M measurements with P_m propagation paths each. A total of 990 indoor planes (walls) of the building have been grouped into 20 different classes of structures. Starting from an initial set of material parameters as initial solution for structure classes, the initial objective function is computed at each new iteration i as

$$C_i = \frac{1}{M}\sum_{m=1}^{M}\frac{1}{P_m}\sqrt{\sum_{n=1}^{P_m}\left((\alpha_{mn})_{\text{mod}} - (\alpha_{mn})_{\text{meas}}\right)_i^2}, \quad (4)$$

where M is the number of conducted measurements, P_m is the number of paths within the measurement m, and α_{mn} are the power taps from (1). The parameters $(\alpha_{mn})_{\text{mod}}$ and $(\alpha_{mn})_{\text{meas}}$ denote the predicted and measured powers of the MPCs, respectively.

4. Measurement Campaign and Calibration Results

4.1. Measurement Campaign. The measurements have been conducted within an indoor office building environment, for which the antenna placements are depicted in Figure 2. In the frequency domain, a vector network analyzer is connected through a GPIB connection to a notebook. It sweeps the channel with a bandwidth of 100 MHz around the central frequency 2.45 GHz. The channel impulse response

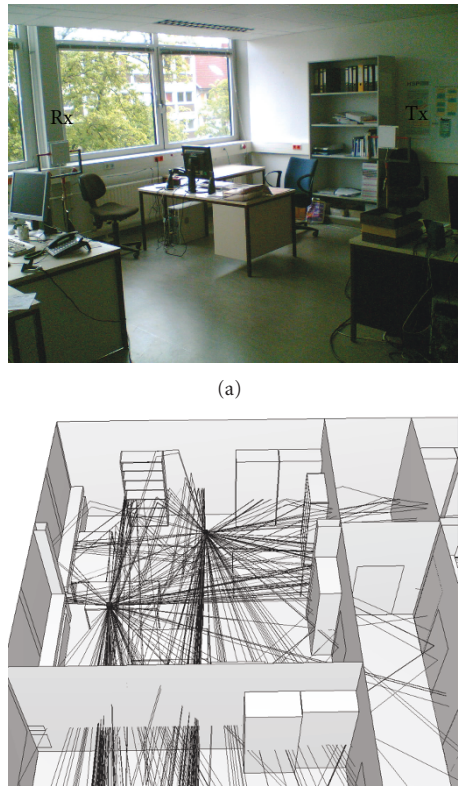

(a)

(b)

Figure 1: (a) A measurement configuration within an office room with (b) a 3D ray tracing.

in the time domain is obtained by the inverse fast Fourier transform (ifft) of the measured complex channel transfer function. In order to overcome the leakage problem of side lobes, while preserving a reasonable pulse width within the channel impulse response, a Hamming window is applied. Two identical WLAN directional antennas, with 14 dBi gain and a half-power beam width of 30°, have been connected to the ports of the VNA via two cables of 10 m length each. The corresponding radiation patterns have been measured in 3D in an anechoic chamber at the frequency of 2.45 GHz and have been introduced into the model. Both antennas can be directed in azimuth and elevation in the range 0–350° with steps of 10° and are positioned at a height level of 1.25 m. Using directional antennas is favorable for focusing the reception on a specific direction targeting a better identification of reflections impinging from the surrounding environment. The performance has been investigated in terms of RMS delay spread (σ_τ [ns]), maximum excess delay ($\tau_{\max}$ [ns]) and path loss (L [dB]), which is computed considering the sum over all MPCs powers above the noise threshold. The channel parameters have been computed considering a noise clipping. A total number of 38 measurements corresponding to 4 transmitter locations, associated with 20 receiver positions on the second floor have been conducted, whereby different antenna tilts (with steps of 90°) have been considered at some positions. These locations are shown in Figure 2. The building database

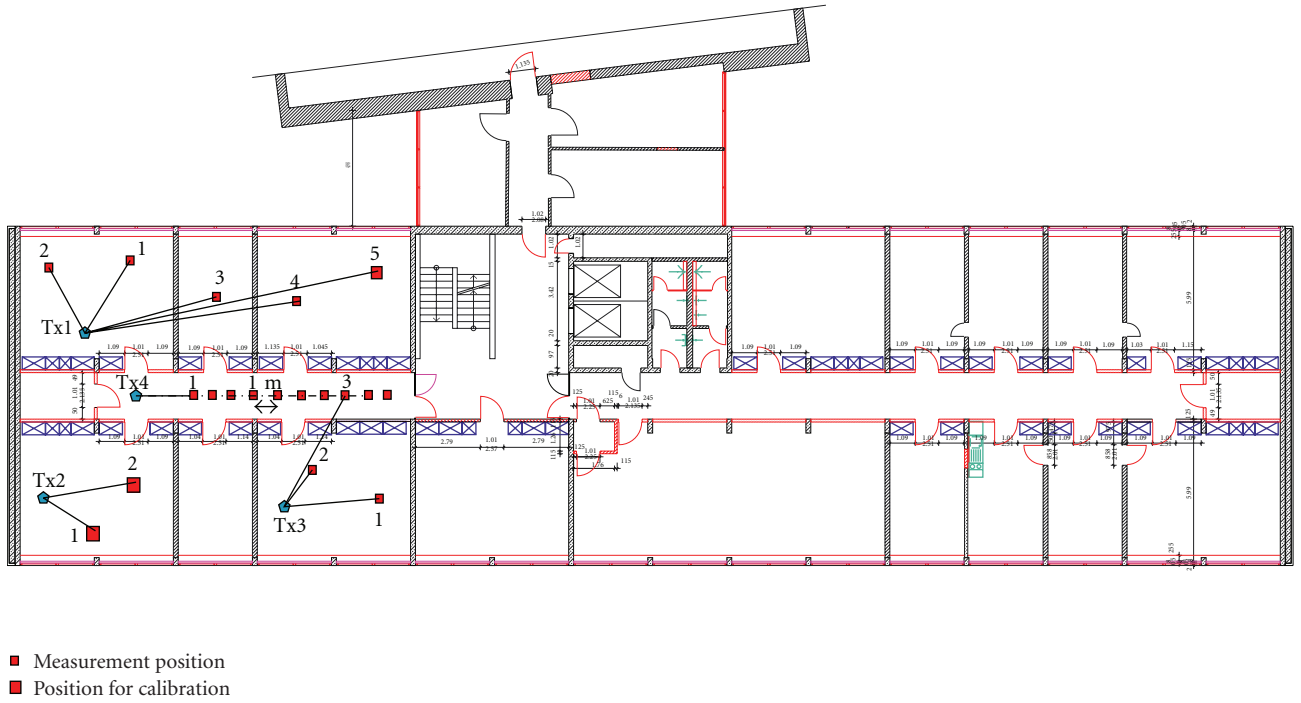

Figure 2: Indoor transmitter and receiver locations.

gathers 900 elementary planes constituting the structures (walls, doors, windiws, cupboards, bookshelves, and tables), as shown in Figure 1.

The offices where the measurements have been conducted are representative of the entire institute building and gather most of the building structures. Moreover, 9 aligned measurements starting at 3 m from the transmitter have been conducted on the floor (as depicted in Figure 2) due to its characteristics enabling LOS conditions and wave-guiding effects.

4.2. Calibration Performance. The calibration has been performed using a set of three measurements for LOS (Tx2-Rx1, Tx2-Rx2) and for NLOS (Tx1-Rx5) as presented in bold squares in Figure 2. Figure 3 displays the PDP (before and after calibration).

The positions Tx2-Rx1 is included in the calibration, Tx1-Rx2 in the neighbor room, and Tx4-Rx1 situated on the corridor are both not used as calibration data. The initial cost function prior to calibration amounts to 5.2 dB, whereas the one after calibration is 1.3 dB. The PDPs have been normalized referring to the direct path power. The good match of the model is resumed in Table 2 regarding channel parameters.

Though initially not included in the calibration, the measurements Tx1-Rx2 and Tx4-Rx1 show a good match with the calibrated model. As expected, the measurement Tx2-Rx1 shows a better match than the other measurements not included in the calibration. However, the advantage of the model resides in providing globally more accurate parameters at any location within the environment without need of huge measurement campaigns to cover the whole building. This is an advantage over the statistical modeling as presented, for example, in [6].

Table 2: Summary of results for the three positions.

Position	Parameter	Measurement	Uncalibrated	Calibrated
Tx2-Rx1	σ_τ [ns]	10.3	2.8	8.1
	$\tau_{\max}$ [ns]	170	60	160
	L [dB]	42.9	44.5	42.2
Tx1-Rx2	σ_τ [ns]	16	5.5	13.8
	$\tau_{\max}$ [ns]	170	70	120
	L [dB]	41.2	43.8	40.4
Tx4-Rx1	σ_τ [ns]	11.8	1.3	7.9
	$\tau_{\max}$ [ns]	160	40	170
	L [dB]	28.8	28.3	28.7

4.2.1. Overall Analysis. An overall improvement of the calibrated model compared to the uncalibrated one is obviously noticeable in most cases. The delay dispersion parameters are considerably improved as the power taps are calibrated. This is demonstrated in Table 3 showing the overall improvement by the new calibrated model in terms of prediction error over all measurements, where the mean, the standard deviation, the minimum, and the maximum error are denoted by $\overline{\Delta}$, Δ_σ, $\Delta_{\min}$, and $\Delta_{\max}$. Hence, the calibrated model delivers globally a significant improvement in characterizing the channel. A mean prediction error of 1.5 dB and a standard deviation of 4 dB are provided by the calibrated model. At a few positions, channel parameters did not improve due to the presence

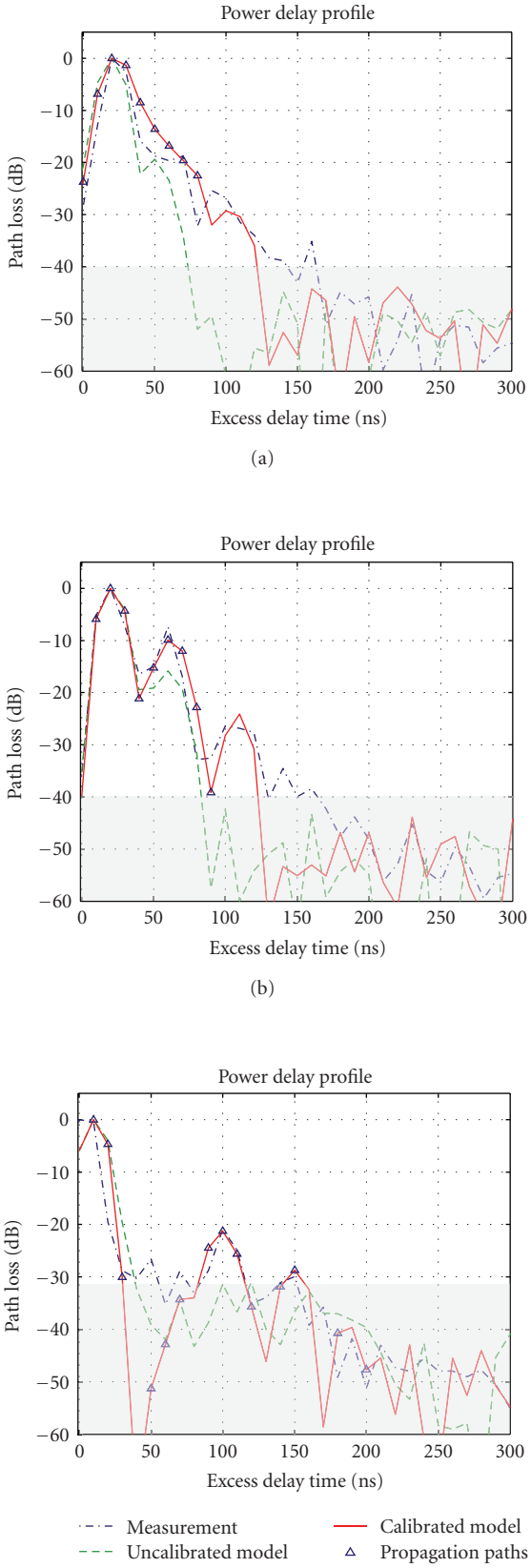

Figure 3: PDP for the measurements (a) Tx2-Rx1 (used as calibration data), (b) Tx1-Rx2 (not used as calibration data), and (c) Tx4-Rx1 (not used as calibration data).

Table 3: Overall prediction error of the model before and after calibration.

Parameter	Statistics	Uncalibrated	Calibrated
σ_τ [ns]	$\overline{\Delta}$	8	4
	Δ_σ	5.1	4.7
	$\Delta_{\min}$	1.5	−5.6
	$\Delta_{\max}$	22.8	18.1
$\tau_{\max}$ [ns]	$\overline{\Delta}$	46	11.9
	Δ_σ	48.1	30.1
	$\Delta_{\min}$	−40	−30
	$\Delta_{\max}$	140	80
L [dB]	$\overline{\Delta}$	1.6	1.3
	Δ_σ	9.1	4
	$\Delta_{\min}$	−23.5	−10.5
	$\Delta_{\max}$	21.1	7.3

Table 4: Path loss prediction error statistics of COST 231 models and calibrated ray tracing.

Model	OSM	MWM	Ray tracing
$\overline{\Delta}$	−5.3	−4.1	1.3
Δ_σ	10.5	9.2	4
$\Delta_{\max}$	26.8	17.8	7.3
$\Delta_{\min}$	−14.8	−17.4	−10.5

of other objects with different materials or due to other propagation mechanisms not considered by the model.

4.2.2. Performance Over COST 231 Models. COST 231 models (one slope model and multiwall model) [12] are narrowband indoor prediction models. These models have been fitted using the same measurements used for the ray tracing. These models are given by the following equations

$$L_{\text{OSM}} = 50.7 + 17.3\,\log(d)\ [\text{dB}], \tag{5}$$

whereas the MWM model is given by

$$L_{\text{MWM}} = 40 + 20\log(d) + c + \sum_w L_w k_w\ [\text{dB}], \tag{6}$$

where the constant loss $c = -6.7$ dB and the wall loss $L_w = 15.7$ dB have been determined by calibration. A comparison of the results of the calibrated model performance over the conventional COST 231 models for all 38 measurements are summarized in Table 4. It is obvious that the calibrated model outperforms the two empirical models. An average error of 1.3 dB is achieved by the ray tracing model, whereas the ones of OSM and MWM remain between −6 and −4 dB. Compared to the COST 231 models, which have a standard deviation between 11 and 9 dB, the calibrated ray tracing model achieves a smaller standard deviation of 4 dB.

Originally, empirical models provide less accuracy compared to ray tracing models, as they only consider the direct path between the transmitter and the receiver. This is the main cause of their weakness especially within a rich multipath indoor environment.

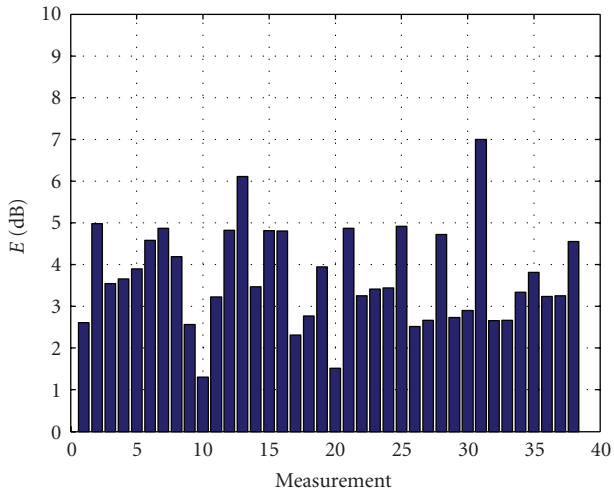

Figure 4: Cost function using one measurement.

5. Sensitivity of the Calibration to the Measurements

Analyzing the performance of the calibration reveals some investigations to be dealt with comprehensively. In this section, the degree of the model performance improvement added by the calibration is assessed as a function of the calibration set size. First, the effect of one measurement is investigated. Subsequently, the impact of increasing the calibration set size has been analyzed.

5.1. Single Measurement-Based Calibration. The optimization on a single measurement is useful to provide an insight into the degree of improvement to be expected with an adequate choice of material parameters. Each of the 38 measurements has been used for calibration of the model and the cost function for this measurement as well as the modeling error are computed for all measurements. Obviously, by virtue of their representative locations in the building, some measurements perform better than others when used for calibration. For instance, measurements 10 and 20 provide the best match with a cost of 1.2 to 1.5 dB (see Figure 4), whereas other measurements (2, 13, and 31) deliver the worst match with an error between 5 and 7 dB.

Each measurement of the 38 has been used singularly for calibration. The overall results of the improvement using one measurement are shown in Figure 5, where $\bar{\varepsilon}$ denotes the absolute average prediction error between the model and the measurements for the complete set of 38 measurements, expressed by

$$\bar{\varepsilon} = \frac{1}{38}\sum_{i=1}^{38} |\Delta_i|, \tag{7}$$

where Δ_i is the prediction error for the ith measurement.

The uncalibrated plot (dashed line) is constant as it is the difference between the measurement and prediction for all the set of data before calibration. It is noticeable that the average error reaches an optimum of 3 dB. However, at some other, less representative locations of the entire building, the calibration results are rather degraded.

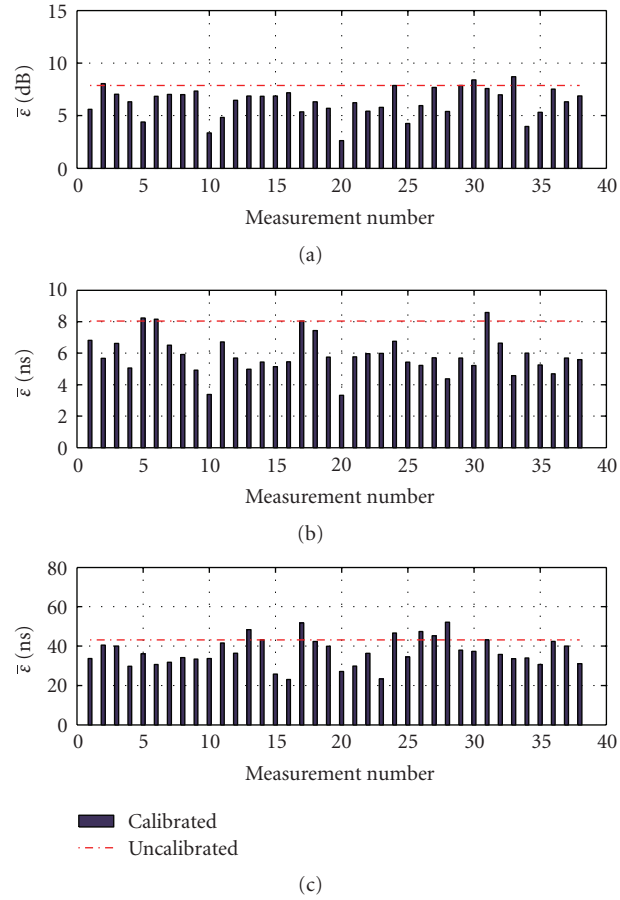

Figure 5: Average error for all measurements with a calibration set of one measurement for (a) path loss, (b) RMS delay spread, and (c) maximum excess delay.

5.2. Measurement Set Size Influence. In order to keep the computation time reasonable with the increasing number of possible combinations, all possible combinations from the first 15 measurements have been considered ($n = 1, \ldots, 15$). The remaining 15 measurements have been added to the set (one each new calibration process) without combination. At each calibration computation, the resulting cost function is recorded and plotted versus the calibration set size (number of measurements) in Figure 6. The cost function undergoes an exponential decay with the variation trend given by the equation in the figure.

Figure 7 shows the average of the errors between the measurements and the calibrated model for all combinations of the 30 measurements, when the number of measurements used to optimize the floor plan is increased. $\bar{\varepsilon}$ denotes the absolute average prediction error for all measurements together. At each calibration process, the calibration set size is incremented by one measurement and the calibration error for all positions is computed. All combinations of measurements have been considered to derive the average

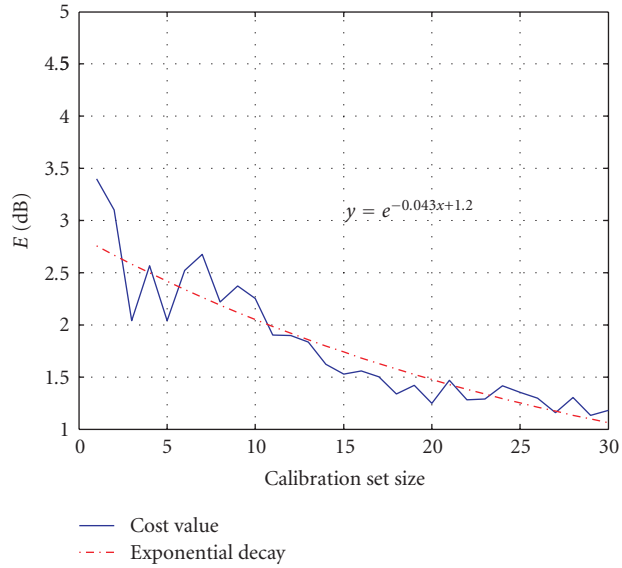

Figure 6: Cost function with increasing size of the calibrating measurement set.

error. The overall degree of improvement in terms of time dispersion and path loss parameters is illustrated in Figure 7.

Henceforth, the remarkable fact which flows from these results is that the error diminishes as the calibration set size increases. This error reaches a fluctuation status around the number of 10, where the modeling error starts to fluctuate around a constant value. This reveals effectively the performance boundary of this deterministic model. It is noteworthy that the prediction error of path loss and time dispersion parameters exhibits a general decay trend with increasing calibration set size. However, a judicious calibration requires a compromise between a best performance and a lower computation time and complexity.

6. Conclusions

This paper addresses the subject of a new deterministic model calibration technique based on simulated annealing, which improves the model performance by means of a few pilot measurements.

The basic facts that emerge from this paper are mainly the model performance improvement and the performance limit reached with more measurements. Indeed, the calibrated model outperforms the standard uncalibrated one with a mean error of 1.3 dB and a standard deviation of 4 dB. With an increasing size of the calibration set, the calibration reaches a steady state for a number of measurements of 10 and starts to deviate around a constant value which shows the performance limit of the ray tracing modeling method. The calibration positions should be chosen in a way to cover the different kinds of rooms in the building in order to enable the coverage of major structures within the environment.

Besides its advantage of compensating for the tedious task of manually tuning the building dielectric parameters plan, the calibration produces an optimized building plan

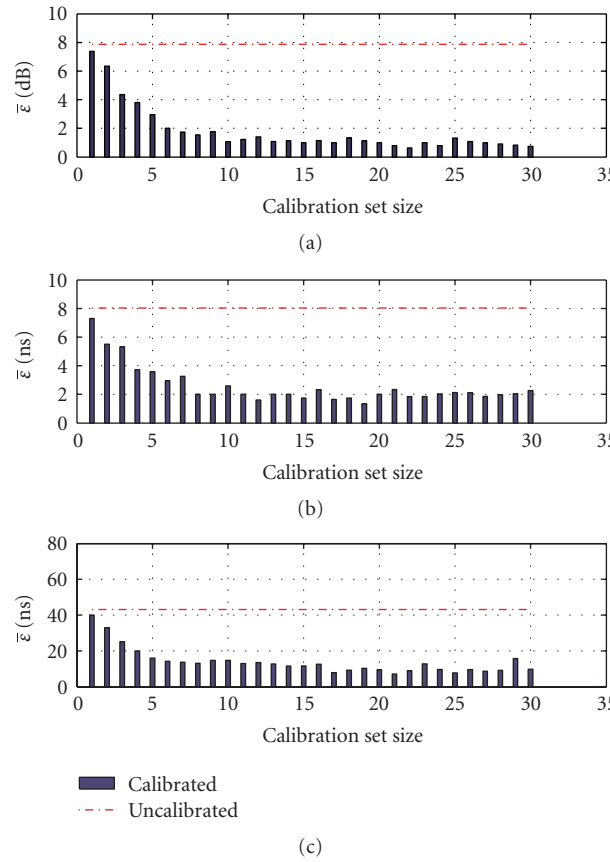

Figure 7: Average error for all measurements in terms of (a) path loss, (b) RMS delay spread, and (c) maximum excess delay with increasing size of the calibrating measurement set.

that works for any conventional ray tracing model. It has been shown that, though the model accuracy improves with an increasing number of measurements used for the optimization, it is indeed bounded and tends to a steady state. The calibration modeling error starts to fluctuate around its extremum after a certain number of measurements, which obviously shows the limits of the deterministic modeling by means of ray tracing.

Directional antennas (as used in this paper) enhance the signal strength and the impinging waves from a certain direction. Omnidirectional antennas can also be used as in [6].

The more the structures a floor plan has the bigger the calibration set size should be in order to optimize all material parameters. Furthermore, the calibrating measurements should involve main propagation paths reflected on the structures to be calibrated.

References

[1] G. Wölfle, *Adaptive Modelle zur Funknetzplanung und zur Berechnung der Empfangsqualität in Gebäuden*, Ph.D. thesis, Institut für Hochfrequenztechnik der Universität Stuttgart, Stuttgart, Germany, 1999.

[2] S. Y. Seidel and T. S. Rappaport, "Site-specific propagation prediction for wireless in-building personal communication

system design," *IEEE Transactions on Vehicular Technology*, vol. 43, no. 4, pp. 879–891, 1994.

[3] J. Beneat and N. Bailey, "Optimization of building material properties for accurate indoor ray tracing models," in *Proceedings of the IEEE Military Communications Conference (MILCOM '04)*, vol. 2, pp. 1010–1014, Monterey, Calif, USA, October-November 2004.

[4] J. Jemai and T. Kürner, "Calibration of indoor channel models," in *Proceedings of the ITG/VDE Mobile Radio Conference, Technologies and Applications*, pp. 31–36, Osnabrück, Germany, May 2007.

[5] J. Jemai and T. Kürner, "Broadband WLAN channel sounder for IEEE 802.11b," *IEEE Transactions on Vehicular Technology*, vol. 57, no. 6, pp. 3381–3392, 2008.

[6] J. Jemai, I. Schmidt, and T. Kürner, "UWB channel: from statistical aspects to calibration-based deterministic modeling," in *Proceedings of the German Microwave Conference (GeMIC '08)*, Hamburg, Germany, March 2008, *European Microwave Journal*. In press.

[7] R. A. Valenzuela, S. Fortune, and J. Ling, "Indoor propagation prediction accuracy and speed versus number of reflections in image-based 3-D ray-tracing," in *Proceedings of the 48th IEEE Vehicular Technology Conference (VTC '98)*, vol. 1, pp. 539–543, Ottawa, Canada, May 1998.

[8] D. A. McNamara, C. W. I. Pistorius, and J. A. G. Malherbe, *Introduction to the Uniform Geometrical Theory of Diffraction*, Artech House, Boston, Mass, USA, 1990.

[9] F. Gil, A. R. Claro, J. M. Ferreira, C. Pardelinha, and L. M. Correia, "A 3D interpolation method for base-station-antenna radiation patterns," *IEEE Antennas and Propagation Magazine*, vol. 43, no. 2, pp. 132–137, 2001.

[10] R. M. Buehrer, A. Safaai-Jazi, W. Davis, and D. Sweeney, "Ultra-wideband propagation measurements and modeling," Final Report, DARPA NETEX Program, Virginia Technology, Blacksburg, Va, USA, January 2004.

[11] H. C. Rhim and O. Büyüköztürk, "Electromagnetic properties of concrete at microwave frequency range," *ACI Materials Journal*, vol. 95, no. 3, pp. 262–271, 1998.

[12] E. Damosso, Ed., "Digital mobile radio towards future generation systems," Cost 231 Final Report, European Commission, Bruxelles, Belgium, 1999, http://www.lx.it.pt/cost231/.